Neurotherapeutics
https://doi.org/10.1007/s13311-020-00865-y

ORIGINAL ARTICLE

Cerebellar Astrocyte Transduction as Gene Therapy for Megalencephalic Leukoencephalopathy

Angela Sánchez[1,2] · Belén García-Lareu[1] · Meritxell Puig[1,2] · Esther Prat[3,4,5] · Jesús Ruberte[6] · Miguel Chillón[1,2,7] · Virginia Nunes[3,4,5] · Raul Estévez[5,8] · Assumpció Bosch[1,2,9]

© The American Society for Experimental NeuroTherapeutics, Inc. 2020

Abstract

Megalencephalic leukoencephalopathy with subcortical cysts (MLC) is a rare genetic disorder belonging to the group of vacuolating leukodystrophies. It is characterized by megalencephaly, loss of motor functions, epilepsy, and mild mental decline. In brain biopsies of MLC patients, vacuoles were observed in myelin and in astrocytes surrounding blood vessels. There is no therapy for MLC patients, only supportive treatment. We show here a preclinical gene therapy approach for MLC using the *Mlc1* knock-out mouse. An adeno-associated virus coding for human MLC1 under the control of the glial fibrillary acidic protein promoter was injected in the cerebellar subarachnoid space of *Mlc1* knock-out and wild-type animals at 2 months of age, before the onset of the disease, as a preventive approach. We also tested a therapeutic strategy by injecting the animals at 5 months, once the histopathological abnormalities are starting, or at 15 months, when they have progressed to a more severe pathology. MLC1 expression in the cerebellum restored the adhesion molecule GlialCAM and the chloride channel ClC-2 localization in Bergmann glia, which both are mislocalized in *Mlc1* knock-out model. More importantly, myelin vacuolation was extremely reduced in treated mice at all ages and correlated with the amount of expressed MLC1 in Bergmann glia, indicating not only the preventive potential of this strategy but also its therapeutic capacity. In summary, here we provide the first therapeutic approach for patients affected with MLC. This work may have also implications to treat other diseases affecting motor function such as ataxias.

Key Words Gene therapy · MLC · cerebellum · myelin · GlialCAM · AAVrh10

Electronic supplementary material The online version of this article (https://doi.org/10.1007/s13311-020-00865-y) contains supplementary material, which is available to authorized users.

✉ Raul Estévez
restevez@ub.edu

✉ Assumpció Bosch
assumpcio.bosch@uab.es

[1] Department of Biochemistry and Molecular Biology and Institute of Neurosciences, Edifici H, Universitat Autònoma de Barcelona, E-08193 Bellaterra, Spain

[2] Unitat Mixta UAB-VHIR, Vall d'Hebron Institut de Recerca (VHIR), Barcelona, Spain

[3] Laboratori de Genètica Molecular, Programa de Genes, Malaltia i Teràpia, IDIBELL, L'Hospitalet de Llobregat, Barcelona, Spain

[4] Unitat de Genètica, Departament de Ciències Fisiològiques, Facultad de Medicina i Ciències de la Salut, Univ. de Barcelona, L'Hospitalet de Llobregat, Barcelona, Spain

[5] Centro de Investigación Biomédica en Red sobre Enfermedades Raras (CIBERER), Instituto de Salud Carlos III, Madrid, Spain

[6] Department of Animal Health and Anatomy and Center of Animal Biotechnology and Gene Therapy (CBATEG), Univ. Autònoma de Barcelona, Barcelona, Spain

[7] Institut Català de Recerca i Estudis Avançats (ICREA), Barcelona, Spain

[8] Departament de Ciències Fisiològiques, IDIBELL - Institute of Neurosciences, Universitat de Barcelona, E-08907 Barcelona, Spain

[9] Centro de Investigación Biomédica en Red sobre Enfermedades Neurodegenerativas (CIBERNED), Instituto de Salud Carlos III, Madrid, Spain

Published online: 05 May 2020

Introduction

Megalencephalic leukoencephalopathy with subcortical cysts (MLC) is a rare type of leukodystrophy characterized mainly by myelin vacuolization and early onset of macrocephaly, appearing at the first year of life [1]. Unsupported walking ability is delayed in MLC1 patients and their gait is unstable [2]. They develop progressive cerebellar ataxia and sometimes spasticity and become wheelchair-dependent as teenagers. Some patients also develop dystonia and athetosis. Mild cognitive deterioration becomes apparent over the years and almost all children have occasional epileptic seizures, often induced by minor head trauma [3]. Some patients have a more severe clinical course, being able to walk without support for only a short time or never achieve it [4]. Unfortunately, no treatment is currently available for MLC patients.

MLC classic phenotype is inherited as autosomal recessive trait and can be caused by mutations in two different genes. The first gene described was *MLC1* (MIM no. 605908) and mutations in this gene cause MLC1-type disease in most patients [5]. The second gene involved in MLC classic phenotype is *GLIALCAM* (MIM no. 611642) [6, 7]. Mutations in *GLIALCAM* can cause two different phenotypes: MLC2A containing recessive mutations and exhibiting the same phenotype as patients carrying mutations in *MLC1* gene [8], and MLC2B inherited in a dominant form. Although MLC2B patients initially have the same symptoms as MLC1 or MLC2A patients, its phenotype improves with time and finally they show different symptoms ranging from a benign form of MLC to macrocephaly and mental retardation with or without autism [7, 9]. *MLC1* encodes for a membrane protein also called MLC1 that is mainly expressed in astrocytes surrounding blood vessels and the Bergmann glia in the cerebellum [10, 11]. Different mutations have been described in *MLC1*, which cause protein degradation [12]. GlialCAM is mainly expressed in astrocytes co-localizing with MLC1, but also in oligodendrocytes [7].

GlialCAM belongs to the immunoglobulin superfamily and it is an adhesion molecule [13]. GlialCAM is needed for MLC1 localization at astrocyte-astrocyte junctions [6, 14]. However, GlialCAM has also been described as an auxiliary subunit of the chloride channel ClC-2 in astrocytes and oligodendrocytes [15], and it is able to modify ClC-2 localization and different functional properties, such as rectification [16]. Lack of *Mlc1* causes GlialCAM and ClC-2 mislocalization in astrocytes and oligodendrocytes, suggesting that trans interactions formed between GlialCAM molecules expressed in these two different cell types may exist [16, 17]. It has been proposed that the mislocalization of GlialCAM and ClC-2 in oligodendrocytes could contribute to the appearance of vacuoles in myelin [16].

Recent studies performed with *Mlc1 and Glialcam* knockout (KO) mice showed the development of macrocephaly and progressive astrocyte and myelin vacuolization in these mice, which were mainly restricted to the fiber tracts of the cerebellum [16, 18, 19]. The vacuolization phenotype progressed very slowly and the animals did not develop the motor or cognitive abnormalities present in humans, thus they are proposed as a model for early MLC phenotype. At 2 months of age, *Mlc1* and *Glialcam* KO animals showed very few vacuoles, which however, became evident at 4 months of age and increased to extensive vacuolization in this area at 1 year of age [16]. Additional loss of *Glialcam* in the *Mlc1* KO did not increase the level of vacuolization [20]. It has been suggested that vacuolization may be caused by defective potassium brain dynamics and/or an alteration of cell volume regulation [21–23].

The precise role of GlialCAM and MLC1 in glial cell ion/water homeostasis is still completely unknown. MLC1 has been related with different homeostatic processes such as the activation of volume-regulated anion currents (VRACs) mediated by the LRRC8 proteins [24, 25], the regulation of the activity of the ClC-2 chloride channel [16], the phosphorylation state of the EGF receptor [26], the regulation of the endosomal pH [27], the response to osmotic stress in cooperation with the TRPV4 channel [28], or the activity of the Na^+/K^+-ATPase [29]. While still looking for the mechanisms of action of these proteins, it is clear that the inactivity or absence of MLC1 or GlialCAM proteins is responsible for the disease phenotype. Thus, providing these proteins to the patient's brain, the normal phenotype may be restored.

In this regard, gene therapy is a promising therapeutic approach for chronic brain diseases since it permits to stably and specifically deliver the missing gene to the target cells, overcoming the difficulty of crossing the blood-brain barrier. Among the available gene delivery vectors, adeno-associated virus (AAV) vectors have several features that make them attractive for brain gene transfer: they are less immunogenic than human adenoviral vectors allowing for long-term transgene expression as recently reported after 15 years of CNS gene transfer in a non-human primate model [30]; they are replication-defective in the absence of helper virus; the wild-type AAV infections are not pathogenic and the vectors do not contain viral genes. Among the AAV serotypes used as gene transfer vectors in preclinical studies, AAV9 and AAVrh10 are the serotypes presenting greater transduction capacity and broader range of cell-type specific tropism, particularly in the CNS. The use of AAVrh10, a non-human serotype, may avoid the neutralization by anti-AAV immune factors present in human sera after natural AAV infections, although cross-reactivity with anti-AAV2, the most common AAV serotype, may still interfere in the therapeutic outcome [31]. Moreover, AAVrh10 is able to transduce glial cells, while AAV9 seems to be more specific for neurons [32].

Particular cell tropism can be efficiently accomplished by combining different AAV serotypes, cell-specific promoters, and different routes of administration, avoiding the non-specific secondary effects caused by conventional pharmacology. *MLC1* gene encodes a protein mainly expressed in glial cells of the adult human brain, such as astrocytes or Bergmann glia with the highest expression in the cerebellum. Glial fibrillary acidic protein (GFAP) is expressed in astrocytes and its promoter has been used to drive exogenous proteins specifically in this cell type in transgenic animals or using viral vectors [33, 34]. Here, we have used AAVrh10 virus containing a GFAP promoter to express human MLC1 in the astrocytes of the cerebellum of *Mlc1*$^{-/-}$ mice at adult stages. We tested different routes of administration and doses to demonstrate that it is possible to restore the localization of GlialCAM and ClC-2 in Bergmann glia after AAV-mediated MLC1 expression specifically in astrocytes and more importantly, to rescue the vacuolation phenotype in *Mlc1* KO, which may have potential as therapeutic gene therapy strategy for MLC patients.

Materials and Methods

Animals

Mlc1 KO animals (*Mlc1*$^{-/-}$) were generated as described previously [16]. KO and wild-type (WT) mice were housed at the Animal Facilities of the IDIBELL, under standard conditions (food and water ad lib, 22 ± 2 °C, 12 h light:dark starting at 08:00), until they were 6 or 12 months old. Experiments and necropsies were performed in the Central Animal Facilities of the Universitat Autònoma de Barcelona. This study was carried out in strict accordance with the current National regulations (Generalitat de Catalunya Decret 214/97 30th July) and with the aim to reduce the number of animals used. The Committees on the Ethics of Animal Facilities of IDIBELL and the Universitat Autònoma de Barcelona approved all procedures described in this study (protocols numbers: DAAM 9073 and CEEAH 2945).

Viral Vector Generation, Production, and Purification

AAVrh10 vectors (null, GFAP-GFP and GFAP-MLC1, with an HA epitope—in bold—AYDR**YPYDVPDYA**MPTL added at the N-terminal region of MLC1 [11]) were produced, purified, and manipulated in the biosafety level 2 facilities of the Vector Production UAB-VHIR Joint Unit (*www.viralvector.eu*) at the Universitat Autònoma Barcelona, Spain. Briefly, vectors were generated using the triple transfection system in HEK293 cells of the expression plasmid (GFAP-GFP or GFAP-MLC1), Reprh10Cap2 plasmid containing AAV genes, and pXX6 plasmid containing adenoviral genes needed as helper virus [35]. After 48 h, AAV vectors were harvested, treated with benzonase, purified in an iodixanol gradient, and titrated using the Picogreen system [36]. Quantification was calculated as viral genomes per milliliter (vg/ml). Control AAVrh10 empty vectors (null) containing only regulatory sequences were used as control.

In Vivo Administration of AAV Vectors

Mice were anesthetized by intraperitoneal injection of ketamine (10 mg/kg of body weight; Imalgene 500; Rhone-Merieux, Lyon-Vénissieux, France) and xylazine (1 mg/kg of body weight; Rompun; Bayer, Leverkusen, Germany). We injected 5×10^{10} vg of each vector by different routes of administration. Intrathecal administration was performed at the lumbar region as previously described [37]. Briefly, after lateral spine exposure by paravertebral muscle dissection, 10 μl of viral vectors was slowly injected into the CSF through a 33-gauge needle and a Hamilton syringe between L3 and L4 lumbar vertebrae. Appropriate access to the intrathecal space was confirmed by tail movement. The needle remained at the injection site for one additional minute after which muscle and skin were sutured. For intracranial administration, animals were mounted onto a stereotactic frame (David Kopf Instruments, Tujunga, CA). Intracerebroventricular administration into the third ventricle was performed at the appropriate coordinates according to *The Mouse Brain Atlas* [38] (ML 1 mm, RC 0.34 mm, DV 2.5 mm) and 5 μl of the vector was administered with an ultramicropump (World Precision Instruments, Sarasota, FL) at a rate of 0.5 μl/min. The needle was slowly withdrawn after additional 5 min. Intracerebellar (ICB) administration was performed in three different ways: ICB into the white matter (ICB WM, 3 μl), ICB into the molecular layer (ICB ML, 3 μl), and ICB in the subarachnoid space (ICB SB, 5 μl). The delivery rate was 0.4 μl/min for intraparenchymal injections and 0.2 μl/min for subarachnoid administration. Coordinates for ICB WM are 0 mm, − 6.24 mm, and 2.5 mm; for ICB ML 0 mm, − 7 mm, and − 1.2 mm; and for IBC SB 0 mm, − 7 mm, and − 0.6 mm (bregma, lateral and depth, respectively). The number of animals injected with each virus, their genotype and gender is listed in Supplementary Table 1.

Immunofluorescence and Histologic Analysis

Anesthetized animals were perfused with phosphate buffer, followed by 4% paraformaldehyde in phosphate buffer. Half brain was embedded with paraffin and the other half was cryoprotected and embedded in Tissue-Tek® O.C.T™ Compound (Sakura FineTechnical Co, Tokyo, Japan). Ten-micrometer-thick sections of sagittal sections were blocked and incubated with primary antibodies overnight at 4 °C. Antibodies against MLC1, GlialCAM, and ClC2 raised in rabbits were

previously described [7, 12, 15]. The following concentrations were used: Anti-MLC1 (1:50), anti-GlialCAM (1:50), anti-ClC-2 (1:100), and anti-GFAP (1:200, Dako, Glostrup, Denmark). Sections were then incubated with the following secondary antibodies: Alexa Fluor goat anti-rabbit 568, goat anti-mouse 568, and goat anti-rabbit 488 (1:200; all from Invitrogen, Carlsbad, CA). Finally, they were counterstained with Hoescht stain solution (Sigma-Aldrich) for nuclei labeling, and they were mounted in Fluoromount (Sigma-Aldrich). Images were acquired using an epifluorescence or a confocal microscope (Leica TCS-SP2 AOBS; Leica Microsystems GmbH, Heidelberg, Germany). The half brain embedded in paraffin was 4-μm-thick sectioned and stained with hematoxylin-eosin and analyzed under bright-field microscope. Morphometric quantification of the number and size of the total number of vacuoles in the white matter was performed in two consecutive slides 40 μm apart, using Image J and Ilastik software [39]. Results were represented as percentage of vacuolated area compared to the total white matter area of each section or as number of vacuoles grouped in 3 different sizes: smaller than 300 μm, from 300 to 500 μm, and larger than 500 μm.

Transmission Electron Microscopic Analysis

Cerebellar fragments of 1 mm^3 were fixed in 2.5% glutaraldehyde and 2% paraformaldehyde for 2 h at 4 °C. After washing in cold phosphate buffer, samples were post-fixed in 1% osmium tetroxide, dehydrated through a graded acetone series, and embedded in epoxy resin. Ultrathin sections (70 nm) from resin blocks were stained using lead citrate and 2% uranyl acetate followed by examination in a transmission electron microscope (H-7000; Hitachi Ltd., Tokyo, Japan).

Western Blot

Some animals were euthanized without perfusion. Half cerebellum was homogenized in membrane extraction buffer (PBS 1 ×, HEPES 25 mM, EDTA 4 mM, sucrose 250 mM) and protease inhibitor cocktail (Millipore, Burlington, MA) and after discarding tissue debris by centrifugation at 4000*g*, cell membranes were obtained by ultracentrifugation at 100,000*g*. Protein concentration was determined by BCA Protein Assay (Pierce, Rockford, IL), and 20 μg of proteins were separated on 10% sodium dodecyl sulfate–polyacrylamide gel electrophoresis (Bio-Rad, Hercules, CA). Polyvinylidene fluoride membranes were incubated with primary antibodies: rabbit anti-human MLC1 (1:1000; [12]) and rabbit anti-GAPDH (1:1000; no. 14C10, Cell Signaling) and secondary antibody anti-rabbit conjugated to horseradish peroxidase (1:2000; DakoCytomation, Glostrup, Denmark) combined with western blotting detection reagent (WESTAR ETA C Ultra 2.0; Cyanagen, Bologna, Italy) according to the manufacturer's instructions.

Quantitative PCR

Total RNA was extracted from the tissue samples using the QIAzol Lysis Reagent (Qiagen, Hilden, Germany), quantified on a NanoDrop spectrophotometer (Thermo Scientific, Waltham, MA), and reverse transcribed into cDNA with iScript cDNA Synthesis Kit (Bio-Rad). Gene-specific primers used for the quantitative PCR analysis were huMLC FW: TCGAGGTAATCGCAGGCATC; huMLC Rv: AGGACCTCCACCAGACACTT; m36B4 Fwd: ATGGGTACAAGCGCGTCCTG; and m36B4 Rv: AGCCGCAAATGCAGATGGAT. Gene-specific mRNA analysis was performed by SYBR green real-time PCR using the MyiQ5 real-time PCR detection system (Bio-Rad). Quantification relative to murine 36B4 controls was calculated using the Pfaffl method [40].

Statistics

Values are represented as mean ± SEM. Statistical analyses using Student's *t* test for qPCR, omnibus analysis by one-way analysis of variance with Tukey *post hoc* tests, and multiple *t* test for each individual size were performed for vacuole size quantification. Differences were considered statistically significant if $p < 0.05$.

Results

Cerebellar Administration in the Subarachnoid Space Is the most Efficient Route to Transduce Bergmann Glia

Recent studies performed with *Mlc1* KO mice showed that they might represent a model of MLC disease at early stages of the disorder, with vacuoles located mainly in cerebellar fiber tracts [16, 18, 19]. Thus, we decided to target the cerebellum of *Mlc1* KO mice as a proof of principle for a gene therapy strategy for MLC. Transduction of the cerebellum is challenging compared to other brain areas. Therefore, we tested several routes of administration using an AAV vector coding for green fluorescent protein (GFP) as a reporter gene, under the regulation of the GFAP promoter, specific for astrocytes (AAV-GFAP-GFP; Fig. 1A).

Animals ($n = 3$ per condition) were injected by lumbar intrathecal puncture (IT, 10 μl), intracerebroventricularly (ICV, 5 μl), or intracerebellarly (ICB) with 5×10^{10} vg of AAV-GFAP-GFP. This later administration was addressed by three different ways, directly in the white matter (WM; 3 μl), or in the molecular layer (ML; 3 μl) or into the CSF in the subarachnoid space (SB; 5 μl) (Fig. 1B). We also tested different delivery speeds, since it has been suggested that the cerebellum could be better transduced by infusing the viruses at low

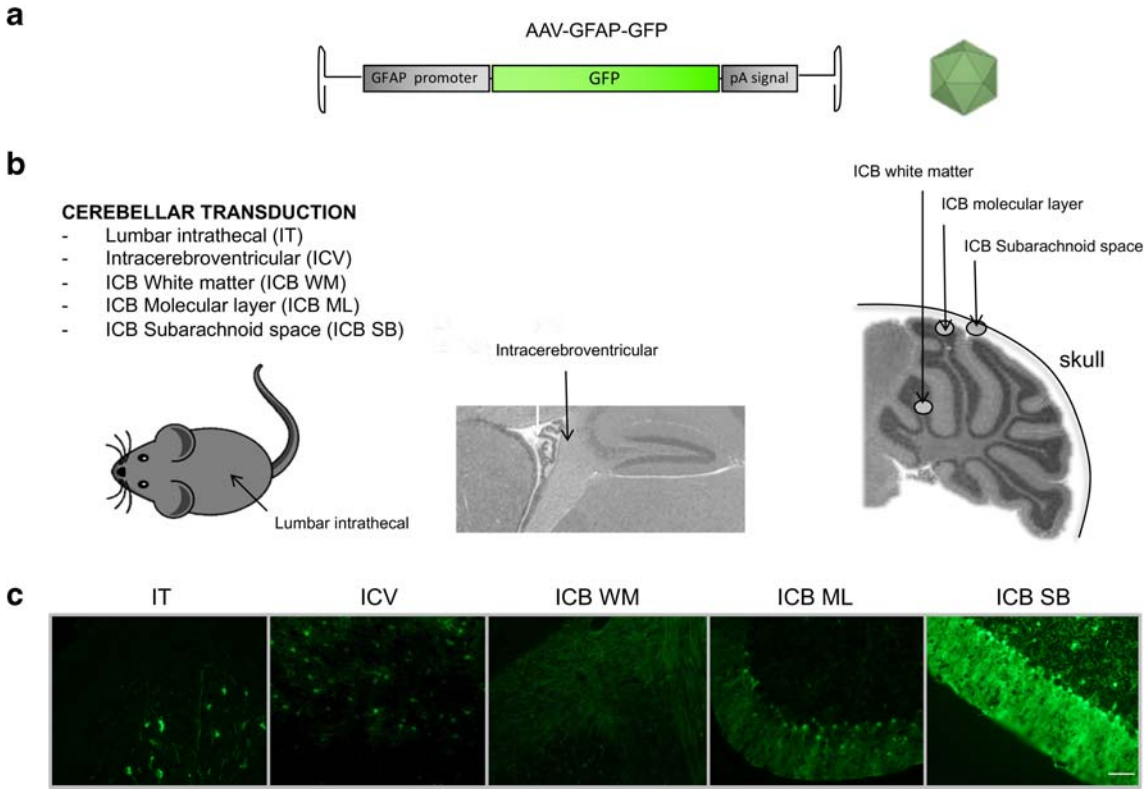

Fig. 1 Intracerebellar administration in the subarachnoid space is the most efficient route to transduce Bergmann glia. (A) Scheme of the viral construct containing GFP as reporter gene under the regulation of the GFAP promoter. (B) Representation of the five administration routes tested in this study. (C) Images were taken using a fluorescence microscope and showed direct GFP fluorescence in the cerebellum of WT animals injected with the AAV-GFAP-GFP by lumbar intrathecal (IT) administration, by intracerebroventricular (ICV) injection, and by intra cerebellar delivery in the white matter (ICB WM), in the molecular layer (ICB ML), or in the subarachnoid space (ICB SB). Scale bar: 100 μm

speed [41]. When animals were administered by lumbar intrathecal injection, GFP expression was observed in the cerebellar white matter but not in the Bergmann glia tracts in the molecular layer (Fig. 1C). By ICV administration, we only detected GFP signal in the contiguous areas of the third ventricle. Finally, ICB WM administration efficiently reached the white matter but the vector did not diffuse to the Bergmann glia. Although ICB ML achieved Bergmann glia transduction, we found that subarachnoid administration of the vector at the cerebellar area (ICB SB) was the most efficient route, achieving high transduction in the whole cerebellum (Supplementary Fig. 1A), both in the white matter and in the Bergmann glia (Fig. 1C, ICB SB), although colocalization with MLC1 was not evident in wild-type animals due to the strong GFP signal that masked MLC1 immunofluorescence (Supplementary Fig. 1B).

Subarachnoid Administration in the Cerebellum of the AAV-GFAP-MLC Vector in *Mlc1* KO Animals Recovers the Expression of MLC1 in Bergmann Glia

A biodistribution study demonstrated that the AAV-GFAP-GFP transduction pattern observed in WT animals replicated in *Mlc1* KO mice ($n = 2$; Fig. 2a). Moreover, when we substituted GFP by human *MLC1* in the AAV vector, MLC1 expression was evident in Bergmann glia in KO animals injected at 2 months of age and analyzed 4 weeks later, as demonstrated by immunohistochemistry ($n = 2$, Fig. 2b–d). Expression in the cerebellum was also corroborated by whole cerebellum quantitative PCR and by Western blot from cerebellar membrane extracts (Supplementary Fig. 2A and B, respectively). In the Western blot, we observed two bands, a lower strong band present only in WT animals, corresponding to the endogenous MLC1, and an upper fainter band, found only in treated animals and compatible with human MLC1 (as it is tagged with a hemagglutinin (HA) epitope).

We initially tested three escalating doses of AAV-GFAP-MLC1: 5×10^9, 2.5×10^{10}, and 5×10^{10} vg/mouse. Two-month-old *Mlc1* KO animals ($n = 3$ per group/dose) were treated before the histopathological symptoms appeared and subsequently analyzed at 8 months of age. Comparing paraffin sections stained with hematoxylin-eosin and consecutive sections immunolabeled with anti-MLC1 antibody, we observed a correlation between the expression of the transgene and the degree of correction of the white matter vacuolation. A complete correction was detected in the medial area with the

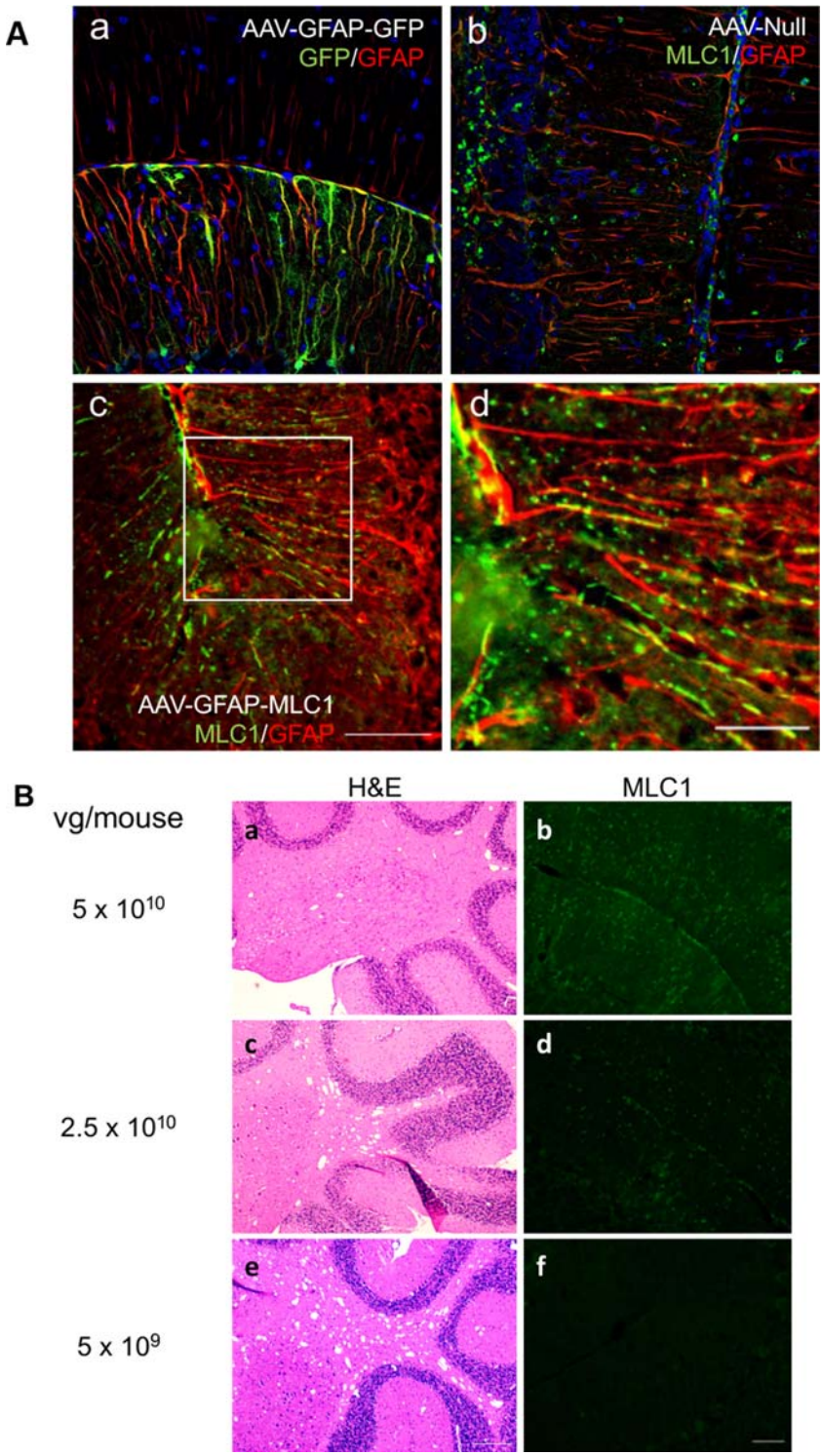

Fig. 2 (A) Subarachnoid administration in the cerebellum of the AAV-GFAP-MLC1 vector in *Mlc1* KO animals recovers the expression of MLC1 in Bergmann glia. (a) GFP expression in Bergmann glia in the cerebellum of *Mlc1* KO animals injected with AAV-GFAP-GFP vector, in green, colocalizes with GFAP astrocytic marker (in red). (b) Undetectable MLC1 expression (in green) in *Mlc1* KO animals injected with the AAV-null vector. GFAP is shown in red. (c) Human MLC1 signal, in green, is detected in Bergmann glia stained in red by GFAP marker after AAV-GFAP-MLC1 administration (scale bar, 50 μm). (d) Inset magnification from c, showing colocalization between MLC1 and GFAP immunoreactivity (scale bar 25 μm). Hoescht co-staining for nuclei is in blue. (B) Correlation between AAV-mediated MLC1 levels and white matter vacuolation. Hematoxylin and eosin staining (left) and consecutive slices with MLC1 immunohistochemistry (in green, right) of the cerebellum from animals injected with different doses of vector. There is a direct correlation between the amount of virus, the immunoreactivity of MLC1 in Bergmann glia, and the number of vacuoles in the white matter of the cerebella. Scale bar: 50 μm in dark-field and 200 μm in bright-field images, respectively

highest dose of viral vector (Fig. 2B, a), which allowed MLC1 expression along the Bergmann glia (Fig. 2B, b). In contrast, many vacuoles were still present with the intermediate dose (Fig. 2B, c), correlating with lower amount of MLC1 expression (Fig. 2B, d). Finally, no differences compared to untreated *Mlc1* KO animals were observed with the lowest dose (Fig. 2B, e), which was not enough to detect MLC1 expression in the transduced animals (Fig. 2B, f).

AAV-null was used as control in *Mlc1* KO and WT mice (n = 3/genotype). As an additional control, we analyzed WT animals injected with AAV-GFAP-MLC1. We did not observe any detrimental effect (measured as an increase in vacuolization, *data not*

shown), contrary to what has been reported in a transgenic animal overexpressing MLC1 [42], suggesting that only supra-physiological levels of MLC1 are deleterious.

MLC1 Administration in Young Animals Prevents the Development of MLC Disease

Considering this preliminary data, we designed a therapeutic study to analyze the potential of our strategy to prevent, treat, or even revert the effects of MLC1 deficiency as schematized in Fig. 3. For that purpose, we injected AAV-GFAP-MLC1 (Fig. 3A) at three different stages of the disease. First, at 2 months of age, previous to disease onset which is around 16 weeks, as a preventive strategy. Second, we injected 5-month-old animals, just after cerebellar vacuolation was evident in this mouse model, as a corrective strategy (early therapeutic approach, Fig. 3B). Both groups of animals were analyzed at 8 months of age, when cerebellar vacuolization has reached its maximum level. And third, we were also interested to check the potential of our strategy to revert the effects of the disease at 15 months of age, 1 year after the development of the first pathological hallmarks of the disease. These animals were analyzed 3 months later, at the age of 18 months (late therapeutic strategy; Fig. 3B).

We compared 3 groups of animals treated at 2 months of age, as a preventive strategy: *Mlc1* KO injected with a null vector, *Mlc1* KO injected with the therapeutic vector carrying the human MLC1 transgene, and as a control, WT animals injected also with the null vector. At 8 months of age, immunohistochemistry for MLC1 showed a substantial increase in their protein signal at Bergmann glia in the treated mice (Fig. 4c) compared to *Mlc1* KO (Fig. 4b), which was very similar to WT animals ($n = 4$; Fig. 4a). Moreover, the mislocalization of GlialCAM and ClC-2 (Fig. 4e and Fig. 4h, respectively) was rescued after treatment with the AAV-MLC1 (Fig. 4f for GlialCAM and Fig. 4i for ClC-2), achieving similar levels to WT animals (Fig. 4d, g). Analogous results were reached in the white matter of treated animals (not shown). We hypothesize that this rescue is not due to mRNA stabilization because it was previously shown that KO of *Mlc1* or *GlialCAM* does not affect mRNA levels of GlialCAM or MLC1, respectively; similarly, ClC-2 mRNA concentration is also unchanged in both KO mice [16]. Our results demonstrated that MLC1 expression is necessary and sufficient to recover the organization of GlialCAM and ClC-2 in *Mlc1* KO mice. The stabilization of ClC-2 and GlialCAM by the reintroduction of MLC1 confirms that the ternary complex formed by the three proteins is more stable at the plasma membrane, as previously seen *in vitro* and *in vivo* [22, 43]. Importantly, restoration of the normal pattern of these three proteins induced also a reduction in the percentage of myelin vacuolization in the cerebellum of 8-month-old animals treated at 2 months of age, when compared to untreated animals (Fig. 4j–l). Thus, restoring expression of MLC1 in the brain with AAV vectors is a preventive treatment in the MLC preclinical mouse model.

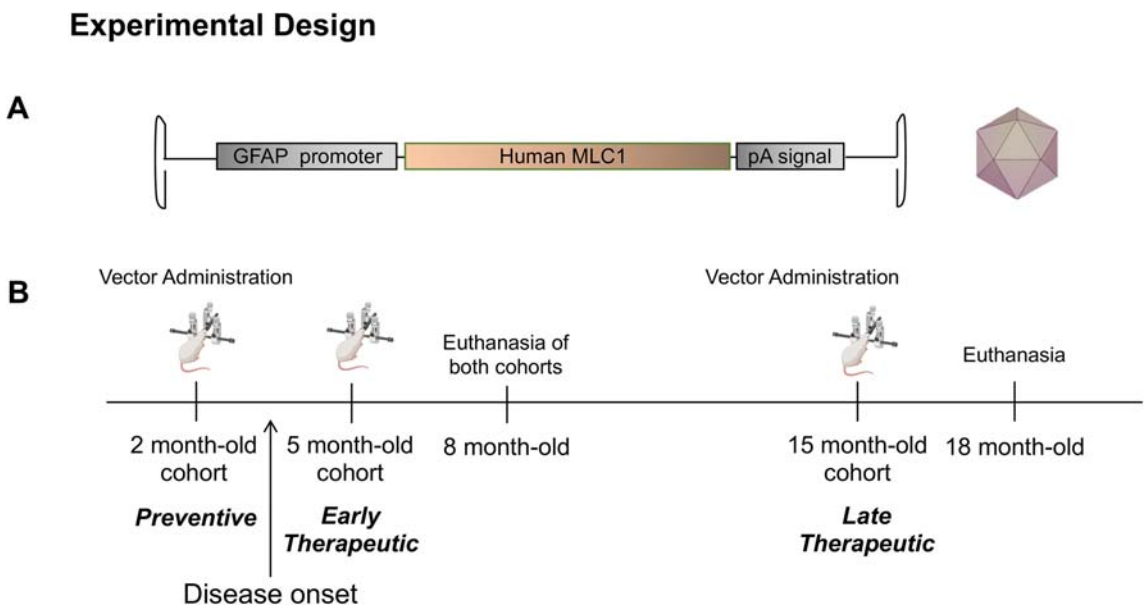

Fig. 3 Experimental design for the gene therapy MLC approach. (A) Scheme of the viral construct containing human *MLC1* as therapeutic gene, under the regulation of the GFAP promoter. (B) Three preclinical studies were designed, the first as a preventive strategy where young non-affected *Mlc1* KO were treated at 2 months and euthanized 6 months later; and two therapeutic studies with animals treated at 5 (early) and 15 months (late) and analyzed 3 months later

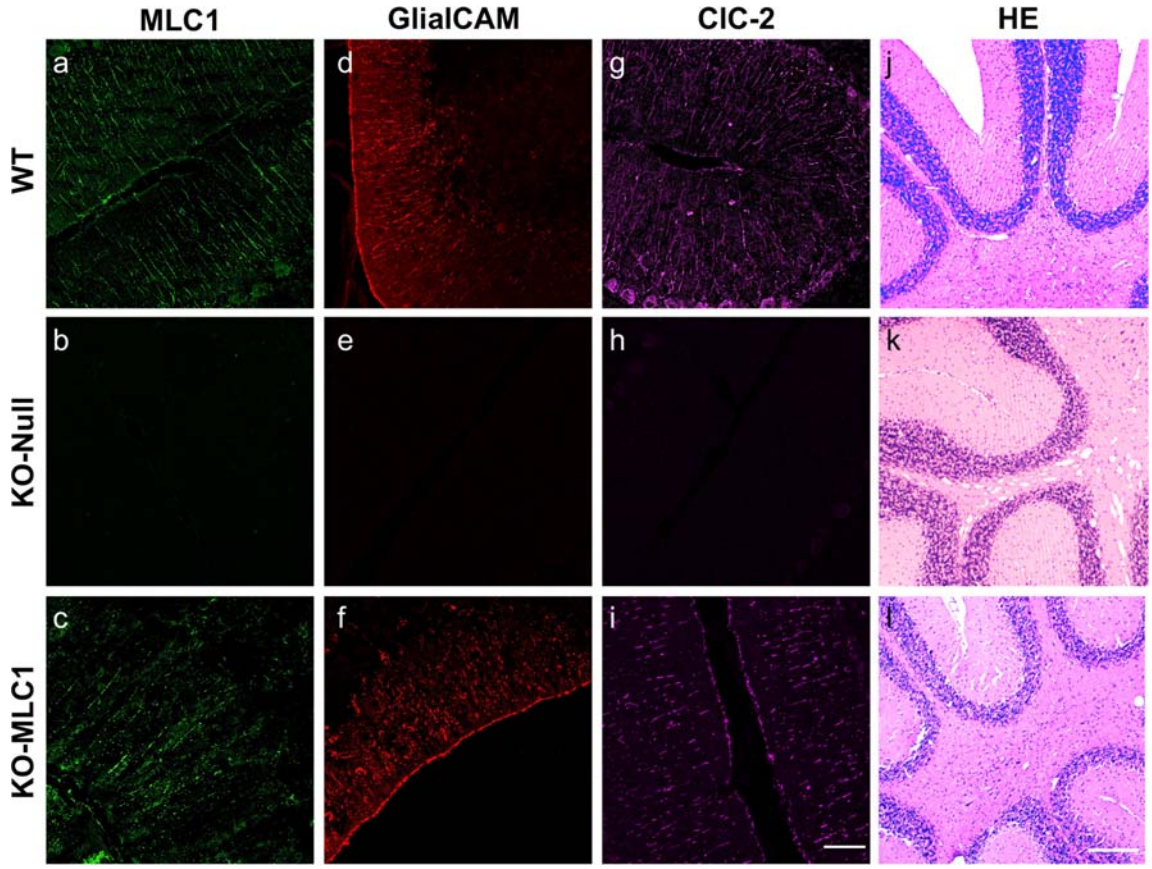

Fig. 4 Human MLC1 transgene expression before disease onset prevents the development of cerebellum vacuolation in *Mlc1* KO animals. (a, d, g) Confocal microscope representative images from WT animals (injected with an AAV-null; $n = 4$) showing MLC1 (a, green), GlialCAM (d, red), or ClC-2 (g, magenta) immunoreactivity. (b, e, h) Confocal microscope representative images from untreated *Mlc1* KO animals (injected with an AAV-Null; $n = 3$) labeled for MLC1 (b, green), GlialCAM (e, red), or ClC-2 (h, magenta). (c, f, i) Immunofluorescence representative images from AAV-GFAP-MLC1-injected KO animals ($n = 4$) labeled for MLC1 (c, green), GlialCAM (f, red), or Clc-2 (i, magenta). Absence of MLC1 and mislocalization of GlialCAM and ClC-2 proteins in *Mlc1* KO animals is evident, and localization of both proteins is restored by the administration of the AAV-GFAP-MLC1 vector. (j, k, l) Representative bright-field microscope images from hematoxylin-eosin staining of untreated WT (j), untreated *Mlc1* KO (k), or treated *Mlc1* KO (l) animals showing a significant reduction of the myelin vacuolation in treated animals, similar to WT. Scale bar: 50 μm in confocal microscopy images and 200 μm in bright-field images

Astrocyte-Directed MLC1 Gene Therapy Significantly Reduces White Matter Vacuoles in the Cerebellum of 5- and 15-Month-Old KO Animals, Demonstrating its Therapeutic Potential

To evaluate the therapeutic potential of this strategy, we treated young but already leukodystrophic *Mlc1* KO animals (at 5 months of age) and followed their recovery up to 3 months after treatment, as a more translational approach. As shown previously, MLC1 expression (Fig. 5a–c) was evident in the Bergman glia of WT and KO-treated animals and correlated with GlialCAM (Fig. 5d–f) and ClC-2 (Fig. 5g–i) expression in the same area. Remarkably, hematoxylin and eosin staining revealed an important reduction in the number and size of the myelin vacuoles in KO-treated animals (Fig. 5j–l).

Finally, to evaluate the potential of reverting MLC pathology with gene therapy, we treated 15-month-old *Mlc1* KO animals, when the disease has already progressed to the most severe pathology, and we analyzed them at 18 months of age. Results are shown in Fig. 6, with very similar histological data as for animals treated before histopathology appeared (2 months of age) or just after it became evident (5-month-old).

Quantification and Ultrastructure Analysis of the Leukodystrophy in MLC1 Mice

To monitor the efficiency of our treatment, we performed an extensive quantification analysis of the vacuolization phenotype. At a first step, we measured the percentage of vacuolated area in 8- or 18-month-old treated animals which was not statistically different from WT mice, while important differences were detected when compared to untreated *Mlc1* KO mice (Fig. 7A). Importantly, quantification of the percentage of vacuolated area was similar between animals injected as before (2 months) or just after histopathology was evident (5 months) and analyzed at the same age.

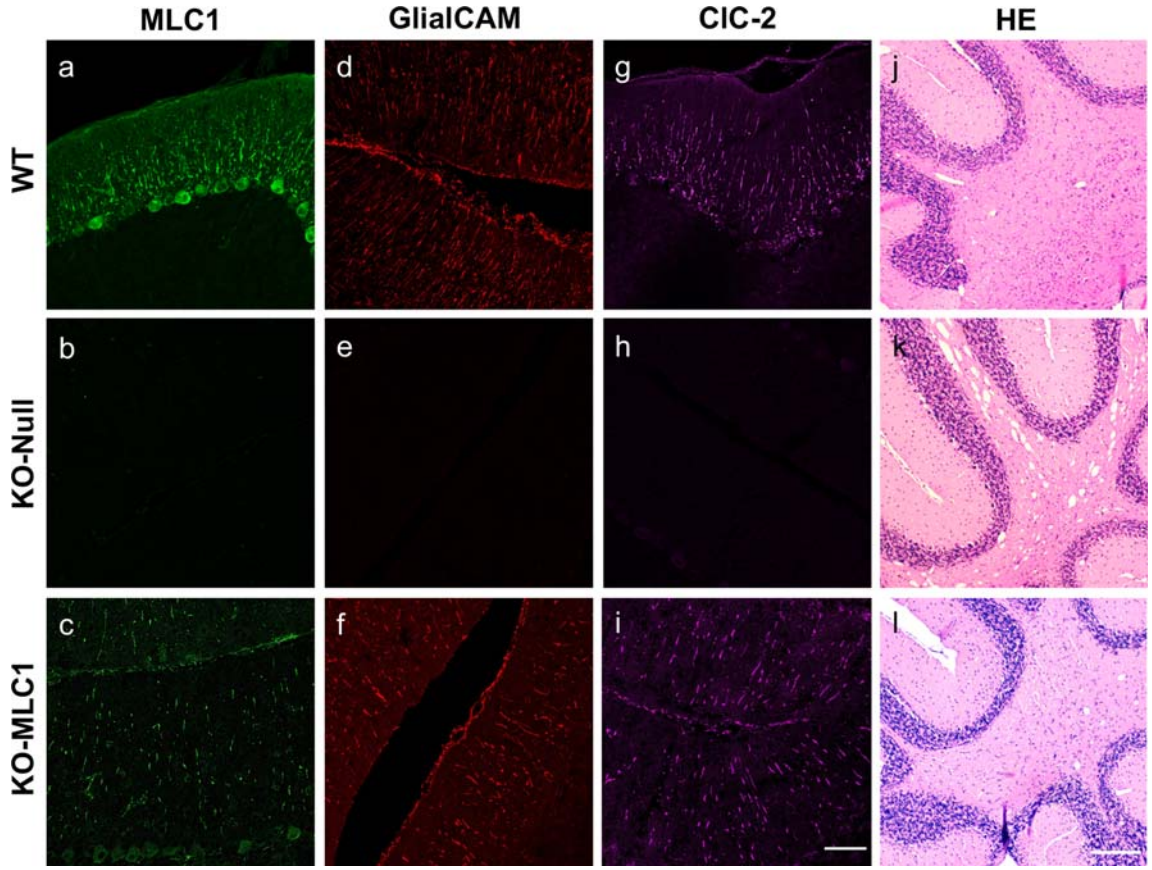

Fig. 5 Human MLC1 administration in disease-affected *Mlc1* KO animals at 5 months of age reduces the vacuolation in cerebellar white matter. (a, d, g) Representative images from WT animals (injected with an AAV-Null; $n = 4$) showing MLC1 (a, green), GlialCAM (d, red), or ClC-2 (g, magenta) immunofluorescence. (b, e, h) Representative fluorescence images from untreated *Mlc1* KO animals (injected with an AAV-null; $n = 3$) showing no immunoreactivity to MLC1 (b, green), GlialCAM (e, red), or ClC-2 (h, magenta). (c, f, i) Representative images from AAV-GFAP-MLC1-injected KO animals ($n = 3$) showing MLC1 (c, green), GlialCAM (f, red), or ClC-2 immunoreactivity (i, magenta). Results indicated a restoration of MLC1, GlialCAM, and ClC-2 localization by the administration of the AAV-GFAP-MLC1 vector in 5-month-old animals similarly to what was observed when animals were treated at 2 months of age. (j, k, l) Representative images from hematoxylin-eosin staining in paraffin sections of WT (j), untreated *Mlc1* KO (k), or treated *Mlc1* KO (l) animals show a significant reduction of the myelin vacuolation in treated animals, as occurred with 2-month-old animals. Scale bar: 50 μm in confocal microscopy images and 200 μm in bright-field images

In a second step, we analyzed the size and number of the vacuoles in these sections. In all size ranges, statistically significant differences were evident between WT and untreated *Mlc1* KO animals (Fig. 7B). Comparing treated and untreated animals, statistically significant differences were also detected for the three treatment groups and vacuole range (Fig. 7B). Moreover, *Mlc1* KO animals in the 8-month-old cohorts did not show any significant differences compared to WT mice and in the group of 18-month-old animals differences were only detected in the smaller size vacuoles ($p < 0.05$) while for sizes larger than 300 μm, late-treated animals were similar to WT mice, reinforcing the therapeutic capacity of the treatment (Fig. 7B).

Finally, we analyzed the ultrastructure of the cerebellar white matter by transmission electron microscopy in 8-month-old *Mlc1* KO mice after 3 months of treatment (Fig. 7C, $n = 2$/group). While large vacuoles in myelin sheaths, mainly affecting oligodendrocytes, extended through the cerebellum in untreated mice (Fig. 7C, a and d), AAV-treated animals showed similar ultrastructure to WT mice (Fig. 7C, b and e vs. c and f). Altogether, this data demonstrate that our strategy is able to revert the phenotype of MLC disease even when it is well established.

Discussion

Despite MLC1 functions are still unknown, we demonstrate here that by restoring MLC1 expression in the cerebellum of Mlc1 KO mice, we can increase the protein levels and rescue the correct localization of GlialCAM and ClC-2 proteins in the Bergmann glia. More importantly, reestablishing the expression of MLC1 leads to a significant decrease of white matter vacuolation, which is a hallmark of MLC. Moreover, there is a

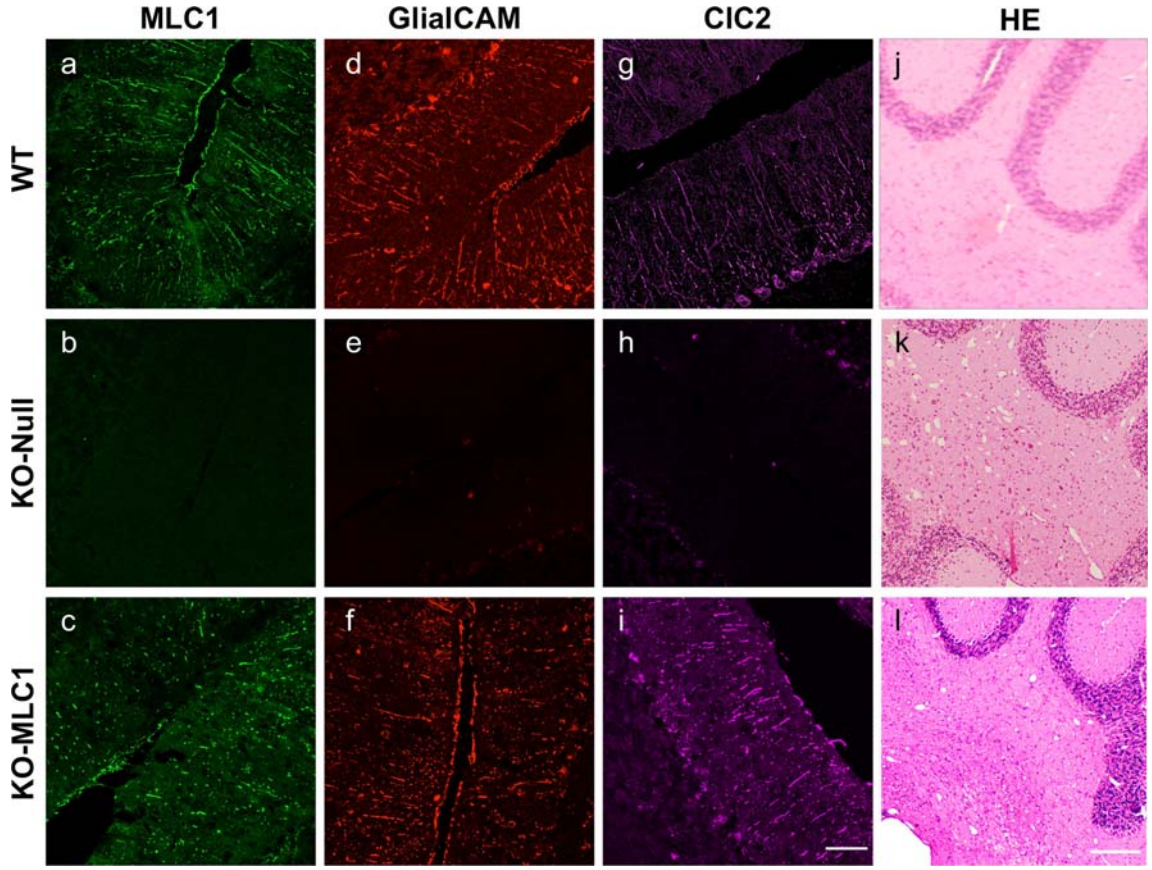

Fig. 6 MLC1 administration in long-term affected *Mlc1* KO mice also reverts the vacuolization phenotype. (a, d, g) Representative images from WT animals (injected with AAV-Null; $n = 3$) showing MLC1 (a, green), GlialCAM (d, red), or ClC-2 (g, magenta). (b, e, h) Representative immunohistochemistry of samples from untreated *Mlc1* KO animals (injected with AAV-null; $n = 4$) showing MLC1 (b, green), GlialCAM (e, red), or ClC-2 (h, magenta) immunoreactivity. (c, f, i) Representative images from AAV-GFAP-MLC1-injected *Mlc1* KO animals ($n = 5$) showing MLC1 (c, green), GlialCAM (f, red), or ClC-2 (i, magenta). (j, k, l) Hematoxylin-eosin staining in paraffin sections of untreated WT (j), *Mlc1* KO (k), or treated *Mlc1* KO (l) animals. Scale bar: 50 μm in confocal microscopy images and 200 μm in bright-field images

correlation between the expression of MLC1 and the number of vacuoles after treatment, although we provide evidence that low levels of MLC1 are enough to diminish the size and the number of myelin vacuoles. This has major implications for therapy for MLC patients, for which there is currently no cure. We are able to restore MLC1 expression in the whole cerebellum, both in Bergmann glia and in the white matter. Interestingly, by correcting MLC1 levels in astrocytes, we significantly reduced the size and number of vacuoles in oligodendrocytes in the white matter. This is probably achieved to a certain extent due to the rescue of GlialCAM location in oligodendrocytes and to the recovery of astrocytic homeostasis.

Gene therapy is a promising therapeutic approach for chronic diseases with brain involvement, since it permits to stably and specifically deliver the missing gene to the target cells, overcoming the difficulty of crossing the blood-brain barrier. The main advantage of the proposed gene therapy strategy is that, by using a particular serotype of AAV vector, a glial-specific promoter, and different routes of administration, we can specifically target astrocytes and avoid non-

Fig. 7 Quantificative and qualitative study of vacuoles in the white matter ▶ of the cerebellum. (A) Percentage of vacuolation was quantified in cerebellar sections separated by 40 μm. Values are expressed as percentage of vacuolated area compared to the total area of the white matter in each section in 8- and 18-month-old animals, WT, treated, or untreated *Mlc1* KO mice ($n = 3$ per age and treatment). One-way ANOVA and Tukey *post hoc* analysis for each time point are depicted on the graph ($^{*}p < 0.05$; $^{**}p < 0.01$). (B) Histogram distribution of vacuoles size (in μm^2) in WT, treated, or untreated *Mlc1* KO mice at 8 and 18 months of age ($n = 3$ per age and treatment). Statistics: omnibus analysis by one-way ANOVA with Tukey *post hoc* tests showed statistical significant differences between WT and KO-null and between treated and untreated KO groups but not between WT and treated cohorts. Multiple *t* tests for the different size range vacuoles show statistically significant differences for all groups and sizes compared with untreated KO ($^{*}p < 0.05$; $^{**}p < 0.01$; $^{***}p < 0.001$) or between small vacuoles from 18-month-old treated vs WT mice ($^{\$}p < 0.05$). (C) Ultrastructural analyses of myelin vacuolization by transmission electronic microscopy. Myelin vacuolization at two different magnifications showing large vacuoles of aberrant myelin in *Mlc1* KO mice (a, d), and normal ultrastructure in *Mlc1* KO mice treated with AAV-GFAP-MLC1 (b, e) and WT animals (c, f). ax, axon; o, oligodendrocyte

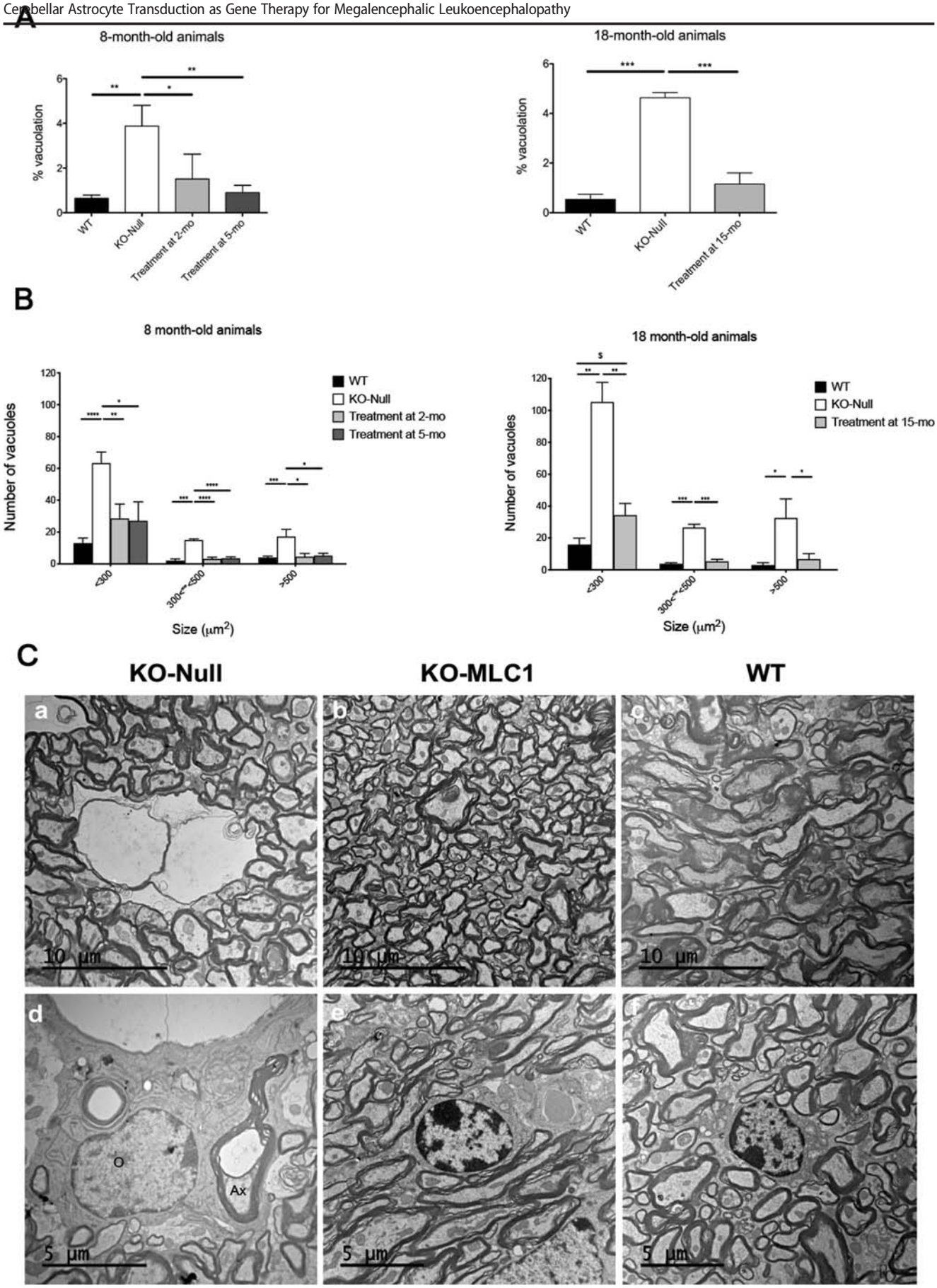
A
8-month-old animals
% vacuolation
WT
KO-Null
Treatment at 2-mo
Treatment at 5-mo
18-month-old animals
Treatment at 15-mo
B
8 month-old animals
Number of vacuoles
Size (μm²)
<300
300<=<500
>500
18 month-old animals
C
KO-Null
KO-MLC1
WT
10 μm
5 μm
Ax

specific effects. Recently, gene therapy in a mouse model of Pelizaeus-Merzbacher-like disease using AAV vectors expressing Connexin 47 in oligodendrocytes resulted in significant phenotypic improvement [44]. Similarly, AAV expressing aspartoacylase in astrocytes were able to rescue the lethal disease phenotype of Canavan disease–affected mice [45].

Mlc1 KO mice, unlike patients with MLC, do not display any motor or cognitive phenotypes, nor do they show changes in the transmission of myelin action potentials [46]. Thus, we used this mouse model at later stages as representative of the MLC disease at its earliest stages, since the mouse myelination pattern is different from that of humans [19]. Very recently, hindlimb clasping when suspended from the tail was reported in a different mouse model of MLC as a sign of neurological abnormality, co-occurring with seizures or increased seizure susceptibility in mouse models for other neurological diseases [21]. We evaluated hindlimb clasping in our mouse model but however no clear abnormality was detected in untreated KO mice which hindlimbs were indistinctly fully spread or fully drown to the abdomen. Thus, no validation of this test could be established for our mouse model.

Expression studies performed during human development suggested that in humans, MLC1 role might be very important at early stages, where protein levels are higher [19]. These results, together with the analysis of a heterozygous knock-in mice [16], explain why patients carrying dominant mutations in *GLIALCAM* have a remitting phenotype: they still have some functional MLC1 localized in astrocyte-astrocyte junctions, and this reduced amount could be enough to perform its function in adulthood, but not in earlier ages. According to this hypothesis, it could be possible to improve the phenotype of MLC patients, even at adult stages. We have demonstrated this hypothesis in long-term affected animals, when the disease has progressed to the most severe phenotype and where we could achieve similar levels of correction than in animals treated as before disease onset or at early stages of the disease.

A recent study in MLC1-overexpressing transgenic mice reported that supra-physiological levels of MLC1 (ten times higher than WT) resulted in white matter cavitation in the brain starting already at postnatal day 7 and continuing up to day 28 [42]. In our hands, no deleterious effects of MLC overexpression were detected in WT animals, suggesting that the levels of MLC1 protein expressed in the cerebellum of KO mice, much lower than WT levels, were sufficient to achieve correction, as expected for a recessive disease, but not detrimental in the WT mice. Nevertheless, an inducible promoter might be used to increase safety.

Translating this strategy to human MLC patients will be challenging but astrocyte-targeted gene therapy with MLC1 has a great potential not only as a preventive treatment, but more importantly for its therapeutic capacity. Global CNS transduction may be necessary since the affected areas are wider than those in the KO mouse, where only the cerebellum is affected. Other routes of administration may be explored like intraventricular or intrathecal administration or its combination with subarachnoid delivery or even convection-enhanced delivery which could allow direct, homogeneous, targeted perfusion of different CNS areas while bypassing the blood-brain barrier [47]. On the other hand, our strategy could open the possibility to treat other diseases affecting the cerebellum.

Acknowledgements We thank Dr. James M. Wilson (University of Pennsylvania, Philadelphia, USA) for providing with AAV Rep2Caprh10 plasmid; Dr. Michael Brenner (University of Alabama, Birmingham, USA) for the GFAP promoter; and Angel Vazquez (UAB) for the technical assistance. This work was supported by the European Leukodystrophy Association (ELA; 2018-00512) to AB, SGR2017-1468 to MC, RTI2018-093493-B-I00 to RE, Hugo Foundation to RE and VN, and FISPI16/00267-R-FEDER and SGR2017-191 to VN. RE is a recipient of an ICREA Academia Prize. VN thanks CERCA Programme/ Generalitat de Catalunya for the IDIBELL support.

References

1. van der Knaap MS, Barth PG, Stroink H et al. Leukoencephalopathy with swelling and a discrepantly mild clinical course in eight children. Ann Neurol 1995; 37:324-334.
2. Singhal BS, Gursahani RD, Udani VP et al. Megalencephalic leukodystrophy in an Asian Indian ethnic group. Pediatr Neurol 1996; 14:291-296.
3. Ben-Zeev B, Gross V, Kushnir T et al. Vacuolating megalencephalic leukoencephalopathy in 12 Israeli patients. J Child Neurol 2001; 16:93-99.
4. Harbord MG, Harden A, Harding B et al. Megalencephaly with dysmyelination, spasticity, ataxia, seizures and distinctive neurophysiological findings in two siblings. Neuropediatrics 1990; 21: 164-168.
5. Leegwater PAJ, Yuan BQ, van der Steen J et al. Mutations of MLC1 (KIAA0027), encoding a putative membrane protein, cause megalencephalic leukoencephalopathy with subcortical cysts. Am J Hum Genet 2001; 68:831-838.
6. Lopez-Hernandez T, Sirisi S, Capdevila-Nortes X et al. Molecular mechanisms of MLC1 and GLIALCAM mutations in megalencephalic leukoencephalopathy with subcortical cysts. Hum Mol Genet 2011; 20:3266-3277.
7. Lopez-Hernandez T, Ridder MC, Montolio M et al. Mutant GlialCAM causes megalencephalic leukoencephalopathy with subcortical cysts, benign familial macrocephaly, and macrocephaly with retardation and autism. Am J Hum Genet 2011; 88:422-432.
8. Hamilton EMC, Tekturk P, Cialdella F et al. Megalencephalic leukoencephalopathy with subcortical cysts: Characterization of disease variants. Neurology 2018; 90:e1395-e1403.
9. van der Knaap MS, Lai V, Kohler W et al. Megalencephalic leukoencephalopathy with cysts without MLC1 defect. Ann Neurol 2010; 67:834-837.
10. Teijido O, Casaroli-Marano R, Kharkovets T et al. Expression patterns of MLC1 protein in the central and peripheral nervous systems. Neurobiol Dis 2007; 26:532-545.
11. Teijido O, Martinez A, Pusch M et al. Localization and functional analyses of the MLC1 protein involved in megalencephalic leukoencephalopathy with subcortical cysts. Hum Mol Genet 2004; 13:2581-2594.

12. Duarri A, Teijido O, Lopez-Hernandez T et al. Molecular pathogenesis of megalencephalic leukoencephalopathy with subcortical cysts: mutations in MLC1 cause folding defects. Hum Mol Genet 2008; 17:3728-3739.
13. Moh MC, Zhang C, Luo C et al. Structural and functional analyses of a novel ig-like cell adhesion molecule, hepaCAM, in the human breast carcinoma MCF7 cells. J Biol Chem 2005; 280:27366-27374.
14. Favre-Kontula L, Rolland A, Bernasconi L et al. GlialCAM, an immunoglobulin-like cell adhesion molecule is expressed in glial cells of the central nervous system. Glia 2008; 56:633-645.
15. Jeworutzki E, Lopez-Hernandez T, Capdevila-Nortes X et al. GlialCAM, a protein defective in a leukodystrophy, serves as a ClC-2 Cl(-) channel auxiliary subunit. Neuron 2012; 73:951-961.
16. Hoegg-Beiler MB, Sirisi S, Orozco IJ et al. Disrupting MLC1 and GlialCAM and ClC-2 interactions in leukodystrophy entails glial chloride channel dysfunction. Nat Commun 2014; 5:3475.
17. Estevez R, Elorza-Vidal X, Gaitan-Penas H et al. Megalencephalic leukoencephalopathy with subcortical cysts: A personal biochemical retrospective. Eur J Med Genet 2018; 61:50-60.
18. Bugiani M, Dubey M, Breur M et al. Megalencephalic leukoencephalopathy with cysts: the Glialcam-null mouse model. Ann Clin Transl Neurol 2017; 4:450-465.
19. Dubey M, Bugiani M, Ridder MC et al. Mice with megalencephalic leukoencephalopathy with cysts: a developmental angle. Ann Neurol 2015; 77:114-131.
20. Perez-Rius C, Folgueira M, Elorza-Vidal X et al. Comparison of zebrafish and mice knockouts for Megalencephalic Leukoencephalopathy proteins indicates that GlialCAM/MLC1 forms a functional unit. Orphanet J Rare Dis 2019; 14:268.
21. Dubey M, Brouwers E, Hamilton EMC et al. Seizures and disturbed brain potassium dynamics in the leukodystrophy megalencephalic leukoencephalopathy with subcortical cysts. Ann Neurol 2018; 83:636-649.
22. Sirisi S, Elorza-Vidal X, Arnedo T et al. Depolarization causes the formation of a ternary complex between GlialCAM, MLC1 and ClC-2 in astrocytes: implications in megalencephalic leukoencephalopathy. Hum Mol Genet 2017; 26:2436-2450.
23. Elorza-Vidal X, Sirisi S, Gaitan-Penas H et al. GlialCAM/MLC1 modulates LRRC8/VRAC currents in an indirect manner: Implications for megalencephalic leukoencephalopathy. Neurobiol Dis 2018; 119:88-99.
24. Capdevila-Nortes X, Lopez-Hernandez T, Apaja PM et al. Insights into MLC pathogenesis: GlialCAM is an MLC1 chaperone required for proper activation of volume-regulated anion currents. Hum Mol Genet 2013; 22:4405-4416.
25. Ridder MC, Boor I, Lodder JC et al. Megalencephalic leucoencephalopathy with cysts: defect in chloride currents and cell volume regulation. Brain 2011; 134:3342-3354.
26. Lanciotti A, Brignone MS, Visentin S et al. Megalencephalic leukoencephalopathy with subcortical cysts protein-1 regulates epidermal growth factor receptor signaling in astrocytes. Hum Mol Genet 2016; 25:1543-1558.
27. Brignone MS, Lanciotti A, Visentin S et al. Megalencephalic leukoencephalopathy with subcortical cysts protein-1 modulates endosomal pH and protein trafficking in astrocytes: relevance to MLC disease pathogenesis. Neurobiol Dis 2014; 66:1-18.
28. Lanciotti A, Brignone MS, Molinari P et al. Megalencephalic leukoencephalopathy with subcortical cysts protein 1 functionally cooperates with the TRPV4 cation channel to activate the response of astrocytes to osmotic stress: dysregulation by pathological mutations. Hum Mol Genet 2012; 21:2166-2180.
29. Brignone MS, Lanciotti A, Macioce P et al. The beta1 subunit of the Na,K-ATPase pump interacts with megalencephalic leucoencephalopathy with subcortical cysts protein 1 (MLC1) in brain astrocytes: new insights into MLC pathogenesis. Hum Mol Genet 2011; 20:90-103.
30. Sehara Y, Fujimoto KI, Ikeguchi K et al. Persistent Expression of Dopamine-Synthesizing Enzymes 15 Years After Gene Transfer in a Primate Model of Parkinson's Disease. Hum Gene Ther Clin Dev 2017; 28:74-79.
31. Thwaite R, Pages G, Chillon M et al. AAVrh.10 immunogenicity in mice and humans. Relevance of antibody cross-reactivity in human gene therapy. Gene Ther 2015; 22:196-201.
32. Petrosyan HA, Alessi V, Singh V et al. Transduction efficiency of neurons and glial cells by AAV-1, -5, -9, -rh10 and -hu11 serotypes in rat spinal cord following contusion injury. Gene Ther 2014; 21:991-1000.
33. von Jonquieres G, Mersmann N, Klugmann CB et al. Glial promoter selectivity following AAV-delivery to the immature brain. PLoS One 2013; 8:e65646.
34. Lawlor PA, Bland RJ, Mouravlev A et al. Efficient gene delivery and selective transduction of glial cells in the mammalian brain by AAV serotypes isolated from nonhuman primates. Mol Ther 2009; 17:1692-1702.
35. Zolotukhin S, Byrne BJ, Mason E et al. Recombinant adeno-associated virus purification using novel methods improves infectious titer and yield. Gene Ther 1999; 6:973-985.
36. Piedra J, Ontiveros M, Miravet S et al. Development of a rapid, robust, and universal picogreen-based method to titer adeno-associated vectors. Hum Gene Ther Methods 2015; 26:35-42.
37. Pages G, Gimenez-Llort L, Garcia-Lareu B et al. Intrathecal AAVrh10 corrects biochemical and histological hallmarks of mucopolysaccharidosis VII mice and improves behavior and survival. Hum Mol Genet 2019; 28:3610-3624.
38. Paxinos G, Franklin, KBJ. The Mouse Brain in Stereotaxic Coordinates, 2nd Edition, 2001. San Diego: Academic Press.
39. Berg S, Kutra D, Kroeger T et al. ilastik: interactive machine learning for (bio)image analysis. Nature Methods 2019; 16:1226-1232.
40. Pfaffl MW. A new mathematical model for relative quantification in real-time RT-PCR. Nucleic Acids Res 2001; 29:e45.
41. Huda F, Konno A, Matsuzaki Y et al. Distinct transduction profiles in the CNS via three injection routes of AAV9 and the application to generation of a neurodegenerative mouse model. Mol Ther Methods Clin Dev 2014; 1:14032.
42. Sugio S, Tohyama K, Oku S et al. Astrocyte-mediated infantile-onset leukoencephalopathy mouse model. Glia 2017; 65:150-168.
43. Gaitan-Penas H, Apaja PM, Arnedo T et al. Leukoencephalopathy-causing CLCN2 mutations are associated with impaired Cl(-) channel function and trafficking. J Physiol 2017; 595:6993-7008.
44. Georgiou E, Sidiropoulou K, Richter J et al. Gene therapy targeting oligodendrocytes provides therapeutic benefit in a leukodystrophy model. Brain 2017; 140:599-616.
45. Gessler DJ, Li D, Xu H et al. Redirecting N-acetylaspartate metabolism in the central nervous system normalizes myelination and rescues Canavan disease. JCI Insight 2017; 2:e90807.
46. Sirisi S, Folgueira M, Lopez-Hernandez T et al. Megalencephalic leukoencephalopathy with subcortical cysts protein 1 regulates glial surface localization of GLIALCAM from fish to humans. Hum Mol Genet 2014; 23:5069-5086.
47. Lonser RR, Sarntinoranont M, Morrison PF et al. Convection-enhanced delivery to the central nervous system. J Neurosurg 2015; 122:697-706.

Publisher's Note Springer Nature remains neutral with regard to jurisdictional claims in published maps and institutional affiliations.